


Article

An Energy-Efficient Adaptive Speed-Regulating Method for Pump-Controlled Motor Hydrostatic Drive Powertrains

Huashuai Wang ^{1,2} , Yanbin Zhang ^{1,3,*}, Zhangshun An ⁴ and Rongsheng Liu ²

¹ School of Mechatronics Engineering, Henan University of Science and Technology, Luoyang 471023, China; huashuai_wang@163.com

² School of Mechanical Engineering, Henan Institute of Technology, Xinxiang 453003, China; rshx1004@163.com

³ Center of Machinery Equipment Advanced Manufacturing of Henan Province, Luoyang 471003, China

⁴ China Railway 11 Bureau Group, Wuhan 430000, China; 18672747100@163.com

* Correspondence: yanbin_zh@haust.edu.cn

Abstract: In this paper, a closed hydrostatic drive powertrain (HSDP) composed of an engine, a variable pump, a variable motor, and an energy-efficient adaptive speed-regulating controller (ADC) based on power following is proposed and investigated. The controller can more than guarantee accurate regulation of motor speed through online efficiency estimation based on established loss models of the pump and the motor. It also facilitates the optimal efficiency control of the engine and hydrostatic system through two redundant control freedoms of the HSDP system, making an energy-saving adjustment of the motor speed. At the same time, the controller can prevent engine overload stall and high system pressure by limiting the displacement of the pumps and motors in real time based on the system loads to improve the automatic adaptability of the system to varying loads. Field testing experiments performed by means of a heavy transportation vehicle under different conditions were conducted to verify the efficacy of the proposed controller. The results showed that the average errors of motor speed were 3.3% under empty load conditions and 9.6% under heavy load conditions. In terms of energy saving, comparison tests involving a rule-based controller (RBC) and the ADC were carried out, and the results showed that the energy-saving ratio of the ADC was at least 11.5% and up to 25.8% under empty load conditions and at least 2.8% and up to 9% under heavy load conditions. The ADC controller showed good performance in terms of speed control, load adaptability, and energy saving and a superior advantage due to its simple structure and ease of implementation. Therefore, the proposed controller is an excellent choice for the real-time control of machinery with an HSDP system, especially heavy-duty machinery.

Keywords: pump-controlled motor; adaptive speed control; energy saving; hydrostatic drive



Citation: Wang, H.; Zhang, Y.; An, Z.; Liu, R. An Energy-Efficient Adaptive Speed-Regulating Method for Pump-Controlled Motor Hydrostatic Drive Powertrains. *Processes* **2024**, *12*, 25. <https://doi.org/10.3390/pr12010025>

Academic Editor: Hsin-Jang Shieh

Received: 25 October 2023

Revised: 12 December 2023

Accepted: 20 December 2023

Published: 21 December 2023



Copyright: © 2023 by the authors. Licensee MDPI, Basel, Switzerland. This article is an open access article distributed under the terms and conditions of the Creative Commons Attribution (CC BY) license (<https://creativecommons.org/licenses/by/4.0/>).

1. Introduction

A pump-controlled motor closed hydrostatic drive powertrain (HSDP) is a common technology used for rotary drives. Due to their advantages in terms of high power density, self-lubrication, simple overload protection, and wide speed regulation range, HSDPs have been widely applied to industrial and construction-related fields [1], such as in heavy manipulators [2], shield machines [3], wheel loaders [4], and heavy transportation vehicles [5]. However, they have also been criticized for their low efficiency and poor emission characteristics [6]. Currently, with the aim of energy saving and emission reduction, energy-saving research on powertrains has attracted great attention from host manufacturers and academic researchers around the world. The use of hybrid power, such as that produced by hydraulic hybrids [7,8], electric hybrids [9], electrohydraulic hybrids [10–12], is one of the main methods for improving the efficiency of powertrains. Its core principle is to adopt the existing or added control freedom of a system to allow the prime mover (engine or electric motor) to work in its high-efficiency region, thus improving the overall efficiency of the transmission system. For example, Ge et al. facilitated the decoupling control of flow and

pump speed through an electrohydraulic power source with variable speed and variable displacement and proposed a strategy of segmented speed and continuous displacement adjustment based on redundant freedom to meet the energy-saving regulation on output flow [13,14]. Wang et al. designed a power split hydraulic torque converter to replace the traditional torque converter on a wheel loader and decoupled the engine and vehicle speeds by controlling the output pressure of the hydraulic torque. Furthermore, with the extra control freedom, energy management strategies were introduced to allow the engine to work in its high-efficiency area [15]. Hippalgaonkar et al. connected a hydraulic pump in parallel with an engine, and an accumulator was added to absorb the extra engine power and assist the engine drive, thus improving the fuel economy of the engine [8]. Kim et al. designed a hybrid powertrain for excavators in which an electric motor was connected in parallel with the engine and an ultracapacitor was employed for energy storage. Moreover, an optimal control strategy based on equivalent fuel consumption was introduced to improve the overall efficiency of the powertrain [9]. Sun et al. proposed a hydraulic and electric synergy hybrid system (HESS) for a heavy-duty vehicle, where a battery and a hydraulic accumulator were installed to assist the engine drive [12]. Aiming to increase the efficiency of hybrid hydrostatic drive vehicles, He et al. comprehensively analyzed the energy losses of each component and the system's overall efficiency in different electrohydraulic hybrid schemes using theoretical and simulation models [16].

Energy management strategies (EMSs) determine how power is distributed between different power sources and loads, rendering them a key factor in improving the efficiency of hybrid powertrains. The core of an EMS lies in the fact that the system can use the extra control freedom of the powertrain to seek optimal control based on rules or optimization results. EMSs can be categorized into two types: optimization-based strategies and rule-based strategies [17]. The optimization-based strategies are designed to seek optimal results using optimization algorithms based on system predictive information and mainly includes model predictive control (MPC) [18], stochastic dynamic programming (SDP) [19], and the Pontryagin's minimum principle (PMP) [20]. The optimization-based strategies can achieve global optimization, but they need predictive information and high-performance control hardware due to their complex calculation processes. The rule-based strategies control a system through a series of predefined rules; these strategies mainly include the thermostatic strategy [21], power-following strategy [22], and fuzzy logic strategy [23]. Although rule-based strategies may not be globally optimal, they have been widely adopted in practical applications due to their simple structure and amenability to implementation in real scenarios.

Extra control freedoms can be obtained for a hybrid powertrain by introducing a new power source into the system. However, in terms of cost, the efficiency improvement brought about by hybrids may not compensate for the cost of the hardware modification of the existing equipment in a short time, especially for machinery with high-power powertrains. As for an HSDP system, the speed of the motor can be adjusted via the engine, the pump displacement, and the motor displacement, resulting in two redundant control freedoms for the system. Therefore, based on the above two redundant freedoms, there is room for fuel economy improvement as long as an EMS can be adopted just as the hybrid powertrains; then, energy-efficient speed control of the motor can be acquired without incurring high modification costs. Backas et al. developed a fuel-optimal controller for an HSDP system based on instantaneous optimization algorithms, and the efficacy of the controller was verified through real-world experiments conducted on a wheel loader [24]. However, this optimal controller requires many control hardware modifications for running complex optimization algorithms. Wen et al. designed a rule-based controller based on power following to control a wheel loader with three closed control loops of vehicle speed, engine speed, and torque; the function of the controller was verified by the simulation results [22]. Unfortunately, the efficacy of the controller in practical applications has yet to be verified. Moreover, for heavy machinery, it will be challenging to achieve stability of the three closed-loop control system for real processes. Zhao et al. proposed a power-matching

strategy for a heavy-duty vehicle to improve its fuel economy. In this method, they adjusted the displacement of the pump and the motor to absorb the available torque of the engine at a certain speed as much as possible; the corresponding energy-saving potential was verified through field tests conducted on the vehicle [25]. However, this strategy considers the energy-saving characteristics of the system more than the speed accuracy of the motor, and the speed control accuracy needs to be further verified. Ye et al. [26] compared different methods for the constant speed control of a variable pump-controlled dual variable motor system, and the simulation results verified the motor speed tracking performance achieved using the two control freedoms. However, the energy-saving characteristics of these control methods were not considered.

This paper presents an adaptive speed-regulating controller (ADC) for an HSDP system based on power following. This controller adopts the two redundant degrees of freedom of an HSDP system to pursue energy-efficient control of the system. The main advantages of the ADC can be described as follows. Firstly, the ADC can pursue energy-saving control by setting the engine and hydraulic components in such a way that they work in their efficient regions. The basic process entails the ADC calculating the set speed of the engine in real time according to the optimal operating curve (OOL) of the engine. Then, according to the actual engine speed and system reference inputs, the ADC sets the displacement of the variable pump and motor based on sequential laws, causing the motor output speed to follow the reference input changes in real time. Secondly, the ADC can also maintain high control accuracy through real-time online efficiency estimation based on established loss models and system feedback signals. Thirdly, the ADC can prevent engine overload stall and high system pressure by limiting the displacement of the pumps and motors in real time based on system loads to improve the automatic adaptability of the system to varying loads. Lastly, the ADC can be easily implemented in practical applications, making it an excellent choice for the energy-saving control of HSDP driving systems. The remainder of this article is as follows. Section 2 describes the structure of the HSDP system and the control methods of the main components. The structure and the working principle of the ADC are introduced in Section 3. Section 4 presents the results of an experimental investigation carried out based on field tests of a heavy transportation vehicle to validate the effectiveness of the ADC. Discussions and future work are presented in Section 5, and conclusions of the work are provided in Section 6.

2. Description of the HSDP System

2.1. Structure and Principle of the HSDP

As shown in Figure 1, the closed hydrostatic drive powertrain (HSDP) is composed of an internal combustion engine (ICE); a variable pump; a variable motor; and other auxiliary systems, such as a charging system, a flushing system, and a safety system.

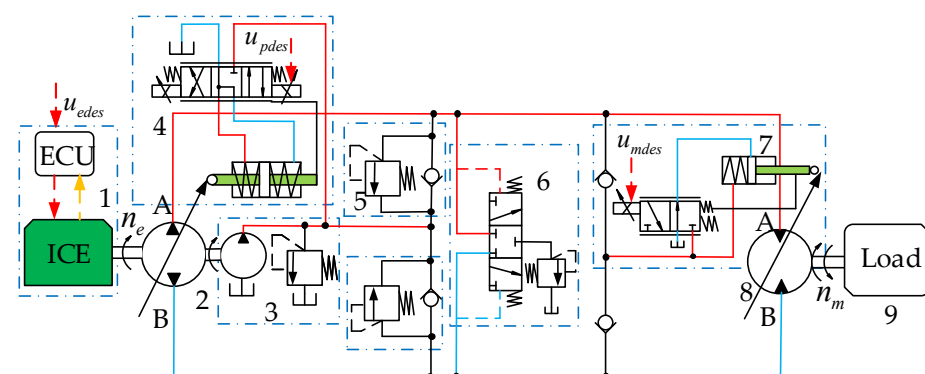


Figure 1. Schematic structure of the HSDP. 1. Internal combustion engine (ICE). 2. Pump. 3. Charging system. 4. Pump displacement control unit (PDCU). 5. Safety valves. 6. Flushing valves. 7. Motor displacement control unit (MDCU). 8. Motor. 9. Load.

The engine (1) directly rotates the pump (2), with the speed being constantly adjusted by the engine controller (ECU). The pump displacement control unit (PDCU) (4) controls the displacement of the pump (2) and the direction of its oil outflow, and the pump (2) outputs oil flow to pipe A or pipe B according to the speed of the engine (1) and the displacement of the PDCU. The motor (8) drives the load (9) in a certain direction under the action of the pressurized oil from the pump (2), with the displacement being regulated by the motor displacement control unit (MDCU) (7). The charging system (3) maintains the low-pressure side of the closed circuit at a certain pressure through oil replenishment to compensate for the loss of the pump (2) and the motor (8). Combined with the charging system (3), the flushing systems (6) exchange the hot oil from the pipe with cooler oil to achieve heat dissipation. The safety system (5) is designed to prevent high system pressure and execute oil replenishment of the low-pressure side of the closed circuit. The control system can achieve stepless adjustment of the output speed of the motor (8) through the three control freedoms of the ICE, PDCU, and MDCU, resulting in two redundant control freedoms.

2.2. Variable Displacement Pump

The outflow q_p (L/min) of the pump is calculated as shown below:

$$q_p = \alpha_p D_{pmax} n_p \eta_{pv} \quad (1)$$

where $\alpha_p \in [-1, 1]$ is the displacement ratio of the pump (for the ease of analysis, only a single direction adjustment of the pump is considered, i.e., $\alpha_p \in [0, 1]$), D_{pmax} (mL/r) is the pump's maximum displacement, n_p is the pump's rotary speed, and η_{pv} is pump volume efficiency.

The electro-proportional control method is used for the PDCU, and its dynamics can be described by a reduced first-order model, as shown in Equation (2):

$$\tau_p \frac{d\alpha_p}{dt} + \alpha_p = u_{pdes} k_{up} \quad (2)$$

where τ_p is the time constant, k_{up} is the control gain, and u_{pdes} (V) is the pump control signal.

In most practical applications, the actual value of α_p is not available due to a lack of displacement sensors; however, its estimated value $\hat{\alpha}_p$ in its discrete form can be obtained based on Equation (2), as shown in Equation (3):

$$\hat{\alpha}_p(k) = \frac{\tau_p}{T_s + \tau_p} \hat{\alpha}_p(k-1) + \frac{k_{up} T_s}{T_s + \tau_p} u_{pdes}(k) \quad (3)$$

where T_s is the sample time of the system (s).

The pump torque T_p (Nm) is calculated as shown below:

$$T_p = \Delta p \hat{\alpha}_p D_{pmax} / 20\pi \eta_{pm} \quad (4)$$

where η_{pm} is the pump's mechanical efficiency, while Δp (bar) is the pressure difference, which can be described as follows: $\Delta p = |p_A - p_B|$.

2.3. Variable Displacement Motor

For simplification, oil compression is ignored, and according to the flow continuity principle, the motor output speed n_m (r/min) is expressed as follows:

$$n_m = q_p \eta_{mv} / \alpha_m D_{mmax} \quad (5)$$

where $\alpha_m \in [0, 1]$ is the motor displacement ratio, D_{mmax} (ml/r) is the motor's maximum displacement, and η_{mv} is the motor's volumetric efficiency.

The reduced first-order model is also used to describe the dynamics of the MDCU.

$$\tau_m \frac{d\alpha_m}{dt} + \alpha_m = u_{mdes} k_{um} \quad (6)$$

where τ_m is the time constant, k_{um} is the control gain, and u_{mdes} (V) is the control signal.

Similarly, according to Equation (6), the estimated value $\hat{\alpha}_m$ of α_m is calculated in discrete form:

$$\hat{\alpha}_m(k) = \frac{\tau_m}{T_s + \tau_m} \hat{\alpha}_m(k-1) + \frac{k_{um} T_s}{T_s + \tau_m} u_{mdes}(k) \quad (7)$$

The motor output torque T_m (Nm) is calculated as shown below:

$$T_m = \hat{\alpha}_m D_{mmax} \Delta p \eta_{mm} / 20\pi \quad (8)$$

where η_{mm} is the motor's mechanical efficiency.

2.4. ICE Module

As shown in Figure 1, as the engine control unit (ECU) conducts closed-loop control of engine speed, the engine speed can be adjusted constantly by only changing the command. Ignoring the influence of the control error and engine droop, the speed control characteristic of the engine can be expressed as follows:

$$\tau_e \frac{dn_e}{dt} + n_e = k_e u_{edes} \quad (9)$$

where n_e (r/min) is the engine speed, τ_e is the time constant, u_{edes} (V) is the engine control signal, and k_e is the control gain.

As the pump shaft is connected directly to the engine, the engine output torque T_e is expressed as follows:

$$T_e = J_e \frac{dn_e}{dt} / 2\pi + T_p + T_{aux} \quad (10)$$

where J_e (Kg · m²) is the equivalent moment inertia of the engine, and T_{aux} (Nm) is the torque required for other systems (cooling, steering, charging, etc.).

3. The Adaptive Controller (ADC)

Figure 2 shows the schematic structure of the adaptive controller (ADC). The ADC is composed of an engine speed set module (ESSM), an efficiency estimation module (EEM), a displacement control module (PMDC), and an adaptive control module (ADCM). The ADC receives more than just the motor reference input n_{mref} from the handle: it also receives system feedback signals, such as the pressure signals p_A and p_B , the engine speed signal n_e , and the motor speed signal n_m . The ESSM calculates the required power of the powertrain based on n_{mref} , $\hat{\alpha}_m$, and Δp and determines the desired speed control signal u_{edes} according to the required power. The EEM provides the estimated system efficiency in real time based on the pump/motor loss models and the system feedback signals. The PMDC sets the pump and motor displacement control signals based on n_{mref} and n_e . The ADCM limits the control signals of the pump and the motor based on the preset pressure difference Δp_{max} and the engine maximum torque to prevent engine overload stall and high system pressure.

Through the cooperative work of the four modules, automatic adaptability to varying loads can be attained along with efficient speed control.

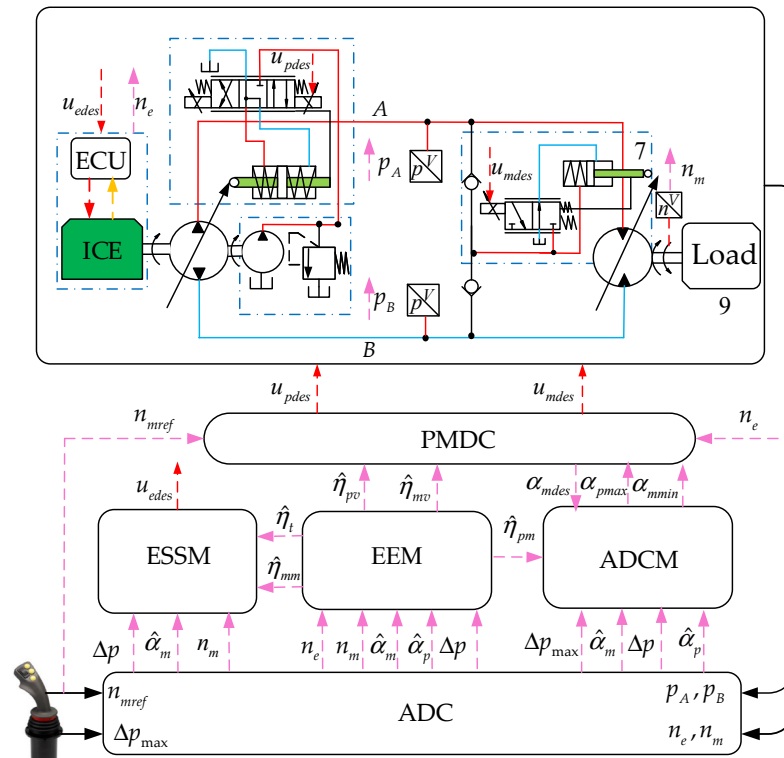


Figure 2. Schematic of the adaptive controller (ADC).

3.1. Efficiency Estimation Module (EEM)

The volumetric efficiency and mechanical efficiency of the pump or motor shows a nonlinear relationship with system pressure, speed, and the displacement ratio [27,28]. In order to improve the accuracy of speed control and power estimation while ensuring the implementation of the system, we conducted real-time online estimation of the efficiencies of the system based on the system feedback signals and the pump/motor loss model. High-fidelity loss models of one specific variable pump and variable motor were established through the response surface method based on the Design-Expert-v8.0 software. The specific application of this software is described in [29]. The loss models of the tested variable pump and motor can be described using the polynomial equations shown in Equations (11)–(16).

The volumetric loss of the variable pump q_{ploss} (L/min) is expressed as follows:

$$q_{ploss} = f_{pq}(\alpha_p, \Delta p, n_p) = 3.645 - 8.14\alpha_p - 2.512e^{-4}n_p + 0.031\Delta p - 5.549e^{-3}\alpha_p n_p - 1.765e^{-3}\alpha_p \Delta p + 9.247e^{-6}n_p \Delta p + 8.088\alpha_p^2 + 1.757e^{-6}n_p^2 - 5.178e^{-5}\Delta p^2 \quad (11)$$

Then, the volumetric efficiency of the variable pump can be estimated in the following manner:

$$\hat{\eta}_{pv} = 1 - q_{ploss} / \hat{\alpha}_p n_p D_{pmax} \quad (12)$$

The mechanical loss of the variable pump T_{ploss} (Nm) can be expressed as follows:

$$T_{ploss} = f_{pT}(\alpha_p, n_p, \Delta p) = 7.173 - 29.677\alpha_p - 0.0391\Delta p + 0.0132n_p + 0.102\alpha_p \Delta p - 2.611e^{-3}\alpha_p n_p - 3.433e^{-6}\Delta p n_p + 25.629\alpha_p^2 + 9.398e^{-6}\Delta p^2 - 3.327e^{-6}n_p^2 \quad (13)$$

The mechanical efficiency of the variable pump can be estimated in the following manner:

$$\hat{\eta}_{pm} = 1 - \frac{T_{ploss}}{\hat{\alpha}_p D_{pmax} \Delta p / 20\pi + T_{ploss}} \quad (14)$$

Similarly, the volumetric loss of the variable motor q_{mloss} (L/min) can be described as follows:

$$q_{mloss} = f_{mq}(\alpha_m, \Delta p, n_m) = -4.028 + 20.991\alpha_m - 2.060e^{-5}n_m - 0.0174\Delta p + 5.012e^{-5}\alpha_m n_m - 0.0354\alpha_m \Delta p + 9.0749e^{-6}n_m \Delta p - 14.002\alpha_m^2 - 3.177e^{-7}n_m^2 + 1.869e^{-4}\Delta p^2 \quad (15)$$

Then, the volumetric efficiency of the variable motor can be calculated as follows:

$$\hat{\eta}_{mv} = 1 - \frac{q_{mloss}}{\hat{\alpha}_m n_m D_{mmax} + q_{mloss}} \quad (16)$$

The mechanical loss of the variable motor T_{mloss} (Nm) can be expressed as follows:

$$T_{mloss} = f_{mT}(\alpha_m, \Delta p, n_m) = 0.719 - 1.407\alpha_m + 9.896e^{-4}n_m + 0.0529\Delta p + 1.771e^{-3}\alpha_m n_m + 0.044\alpha_m \Delta p - 1.57e^{-5}n_m \Delta p \quad (17)$$

The mechanical efficiency of the variable motor can be determined as follows:

$$\hat{\eta}_{mm} = 1 - \frac{T_{mloss}}{\hat{\alpha}_m D_{mmax} \Delta p / 20\pi} \quad (18)$$

The estimated overall efficiency of the hydrostatic system is calculated as follows:

$$\hat{\eta}_t = \hat{\eta}_{pv} \hat{\eta}_{mv} \hat{\eta}_{pm} \hat{\eta}_{mm} \quad (19)$$

The scaling law can be applied to the loss models of a pump and motor of the same type but different sizes [30]. Then, the scaling factor λ is introduced to appropriately scale the speed, flow, displacement, and torque of the pump and the motor to extend them to the application range of the established loss models. The scaling law can be described using Equation (20) through to Equation (23).

$$\lambda = \left(\frac{D_i}{D_{ref}} \right)^{\frac{1}{3}} \quad (20)$$

$$n_i = \lambda^{-1} n_{ref} \quad (21)$$

$$q_i = \lambda^2 q_{ref} \quad (22)$$

$$T_i = \lambda^3 T_{ref} \quad (23)$$

where D_i and D_{ref} are the rated displacement of the applied and tested pump or motor, respectively.

3.2. Engine Speed Set Module (ESSM)

Brake-specific fuel consumption (BSFC) is a measuring index of engine fuel economy; the lower the value, the better the fuel economy. Figure 3 shows the universal characteristic curve of a certain engine; it can be seen that the BSFC is different under different speeds and different loads, and its minimum value is reached when the load torque is close to the maximum torque at the current speed. Therefore, for each engine speed n_e , there is an engine power level P_{emax} with minimum BSFC. Then, the engine optimal operating curve (OOL) can be created by connecting these points (n_e, P_{emax}) , as shown in Figure 3. Using the polynomial fitting method, the relationship between n_e and P_{emax} is expressed as follows:

$$n_e = B_0 + B_1 P_{emax} + B_2 P_{emax}^2 + B_3 P_{emax}^3 \quad (24)$$

where $B_0 \sim B_3$ are the fitting coefficients.

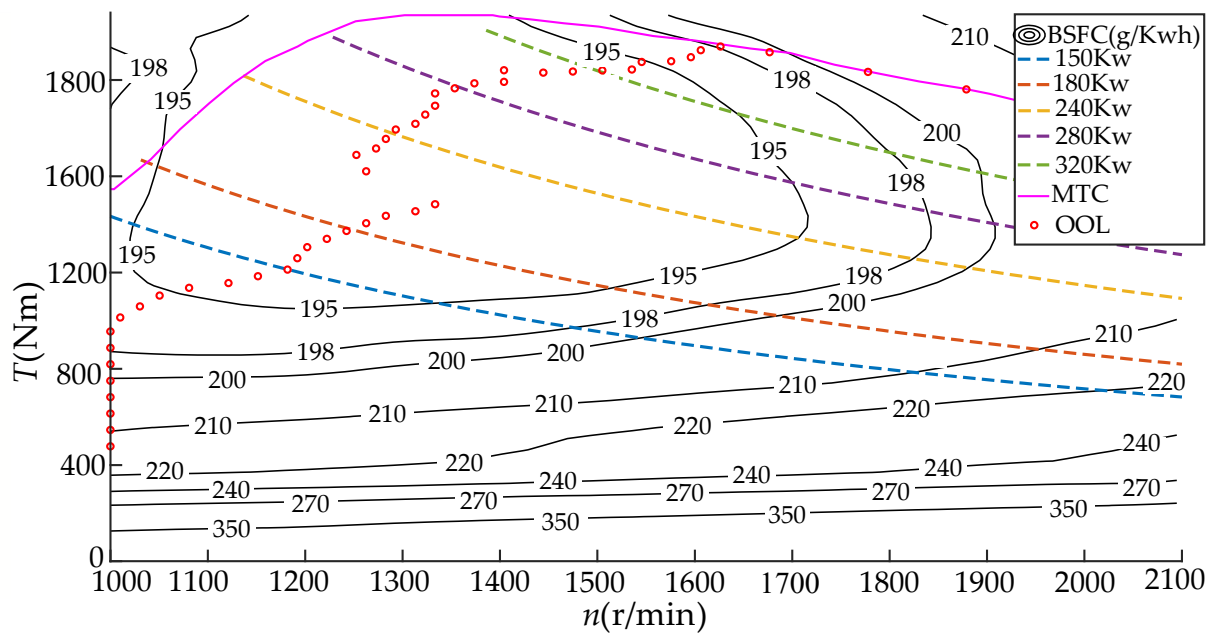


Figure 3. Universal characteristic map of the engine.

Taking the minimum speed requirement of the pump and other systems into consideration while avoiding the frequent speed adjustment of the engine, we designed a sub-optimal engine operating curve (Sub-OOL) based on segmented speed control, as shown in Figure 4.

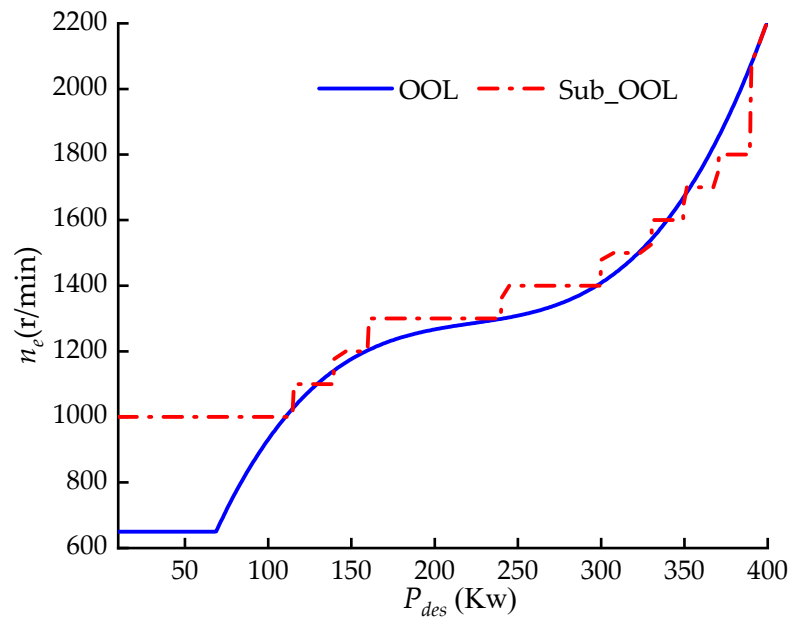


Figure 4. Segmented speed control of the engine.

Using the motor reference speed n_{mref} , the system feedback differential pressure Δp and the estimated $\hat{\alpha}_m$ and $\hat{\eta}_t$, the real time desired engine power P_{edes} (Kw) can be calculated as follows:

$$P_{edes} = \frac{2\pi T_m n_{mref}}{60000 \hat{\eta}_t} = \frac{\hat{\alpha}_m D_{mmax} \Delta p \eta_{mm} n_{mref}}{600000 \hat{\eta}_t} \quad (25)$$

Based on the desired engine power P_{edes} , the desired engine speed n_{edes} can be determined according to the Sub-OOL curve (shown in Figure 4). Then, referring to Equation (9), the desired engine speed control signal u_{eds} can be expressed as follows:

$$u_{eds}(k) = \frac{(T_s + \tau_e)n_{edes}(k) - \tau_e n_{edes}(k-1)}{k_e T_s} \quad (26)$$

3.3. Displacement Control Module (PMDC)

Previous studies have systematically analyzed the efficiency of closed hydrostatic systems and pointed out that in most working areas, the efficiency of a hydrostatic system increases with the increase in the displacement of the pump and the motor [31–33]. Accordingly, in this paper, we propose a displacement control strategy based on sequential logic control. This strategy is as follows: when the desired pump displacement ratio α_{pdes} does not reach its maximum α_{pmax} , then maintain the desired motor displacement ratio α_{mdes} at its maximum value 1 and regulate the motor speed by adjusting α_{pdes} based on n_{mref} ; furthermore, after α_{pdes} reaches up to α_{pmax} , maintain α_{pdes} at α_{pmax} and regulate the motor speed through adjusting α_{mdes} according to n_{mref} .

According to the flow continuity equation obtained with Equations (1) and (5), the sequential control logic of the PMDC can be described by Equation (27):

$$\alpha_{pdes} = \begin{cases} \frac{n_{mref} \alpha_{mmax} D_{mmax}}{\hat{\eta}_{pv} \hat{\eta}_{mv} n_e D_{pmax}} & \alpha_{pdes} < \alpha_{pmax}; \\ \alpha_{pmax} & \alpha_{pdes} \geq \alpha_{pmax}; \end{cases} \quad (27)$$

$$\alpha_{mdes} = \begin{cases} 1 & \alpha_{pdes} < \alpha_{pmax}; \\ \frac{n_e \alpha_{pmax} D_{pmax} \hat{\eta}_{mv} \hat{\eta}_{pv}}{n_{mref} D_{mmax}} & \alpha_{pdes} \geq \alpha_{pmax}; \\ \alpha_{mmin} & \alpha_{mdes} \leq \alpha_{mmin}; \end{cases}$$

Herein, α_{pmax} , α_{mmin} are the upper limit of the pump displacement ratio and the lower limit of the motor displacement ratio, respectively, which are to be determined via the ADCM in the next section. To be specific, Figure 5 shows the control law of α_{pdes} and α_{mdes} under different n_e and n_{mref} .

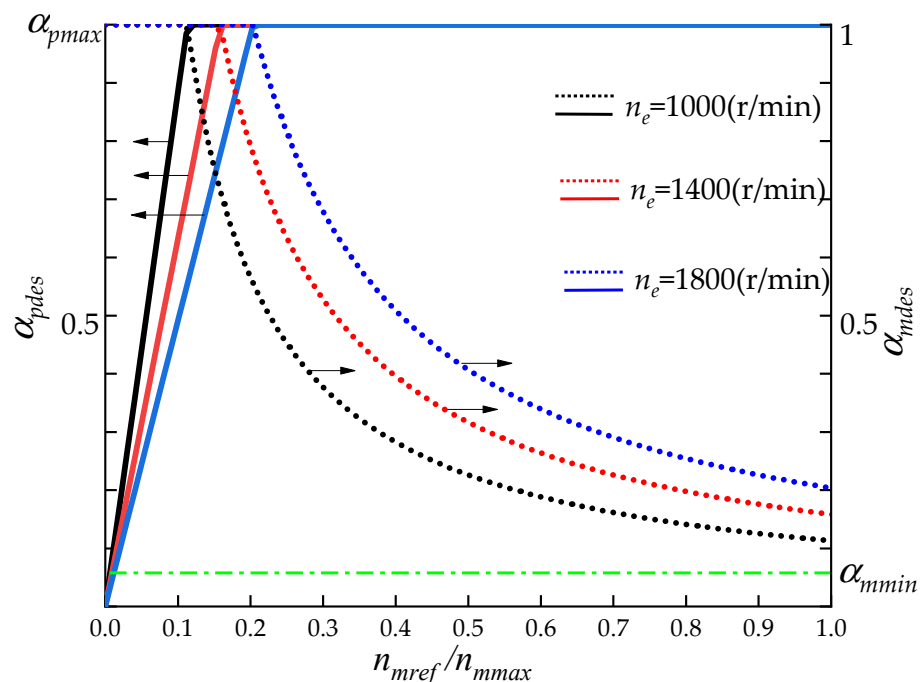


Figure 5. Control law of α_{pdes} and α_{mdes} .

According to Equation (3), the desired pump control signal u_{pdes} is calculated as follows:

$$u_{pdes}(k) = \frac{(T_s + \tau_p)\alpha_{pdes}(k) - \tau_p\alpha_{pdes}(k-1)}{k_{up}T_s} \quad (28)$$

Similarly, according to Equation (7), the desired motor control signal u_{mdes} is calculated as follows:

$$u_{mdes}(k) = \frac{(T_s + \tau_m)\alpha_{mdes}(k) - \tau_m\alpha_{mdes}(k-1)}{k_{um}T_s} \quad (29)$$

3.4. Adaptive Control Module (ADCM)

Figure 3 shows the max torque curve (MTC) of the engine, and it can be seen that there is a maximum output torque T_{emax} at each engine speed n_e , beyond which the load will lead to engine speed droop or engine stall. The polynomial fitting method was also adopted to establish the relationship between T_{emax} and n_e , as expressed in Equation (30):

$$T_{emax}(n_e) = C_0 + C_1n_e + C_2n_e^2 + C_3n_e^3 \quad (30)$$

Here, $C_0 \sim C_3$ are the fitting coefficients.

Combining Equation (4) with Equation (10) and ignoring the torque demand of other systems, the torque relationship between the engine and the pump under steady-state conditions can be approximately expressed as follows:

$$T_e \approx T_p = \Delta p \hat{\alpha}_p D_{pmax} / 20\pi\eta_{pm} \quad (31)$$

In order to ensure the engine abilities of overload resistance and acceleration while taking into account the actual torque needs of other systems (cooling, charging, steering, etc.), 80% of the maximum torque T_{emax} was selected as the available torque T_{eava} for the HSDP system.

The ADCM is capable of more than just limiting the maximum engine output torque by limiting α_{pmax} of the pump to prevent engine speed droop or engine stall; it can also avoid high system pressure by limiting the minimum displacement ratio α_{mmin} of the motor, thus improving the automatic adaptability of the HSDP system to varying loads.

To maintain the engine torque so it does not exceed its available T_{eava} under a certain speed, based on Equations (30) and (31), the real-time α_{pmax} of the pump can be calculated by Equation (32). Figure 6 shows the variation of α_{pmax} with pressure difference Δp and engine speed n_e .

$$\alpha_{pmax} = \begin{cases} 1 & \alpha_{pmax} \geq 1; \\ \frac{2\pi\eta_{pm}T_{eava}(n_e)}{D_{pmax}\Delta p} & \alpha_{pmax} < 1; \end{cases} \quad (32)$$

The predefined maximum pressure difference Δp_{max} and the control gain k_p are introduced to limit the system maximum pressure according to Equation (8), and the real-time α_{mmin} of the motor can be calculated by Equation (33). Figure 7 shows the variation of α_{mmin} with pressure difference Δp and the desired motor displacement ratio α_{mdes} :

$$\alpha_{mmin} = \begin{cases} 1 & \alpha_{mmin} \geq 1; \\ \frac{k_p\Delta p}{\Delta p_{max}}\alpha_{mdes} & \alpha_{mmin} < 1; \end{cases} \quad (33)$$

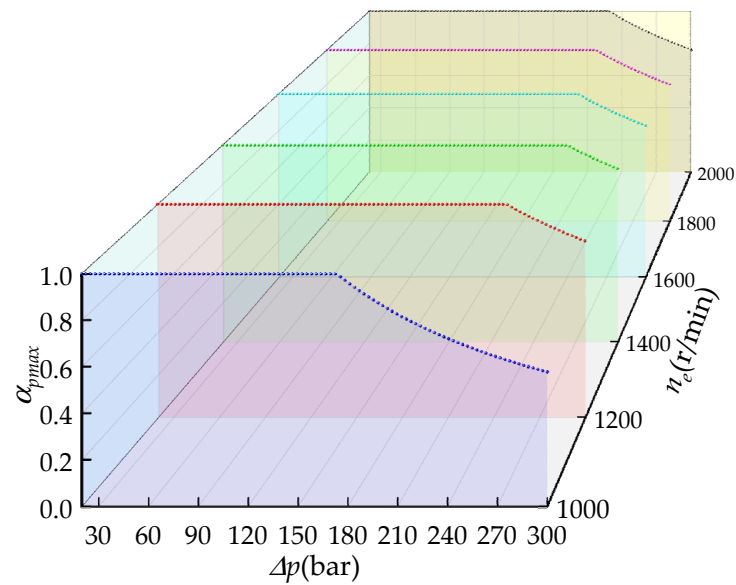


Figure 6. Variation in α_{pmax} under different values of Δp and n_e .

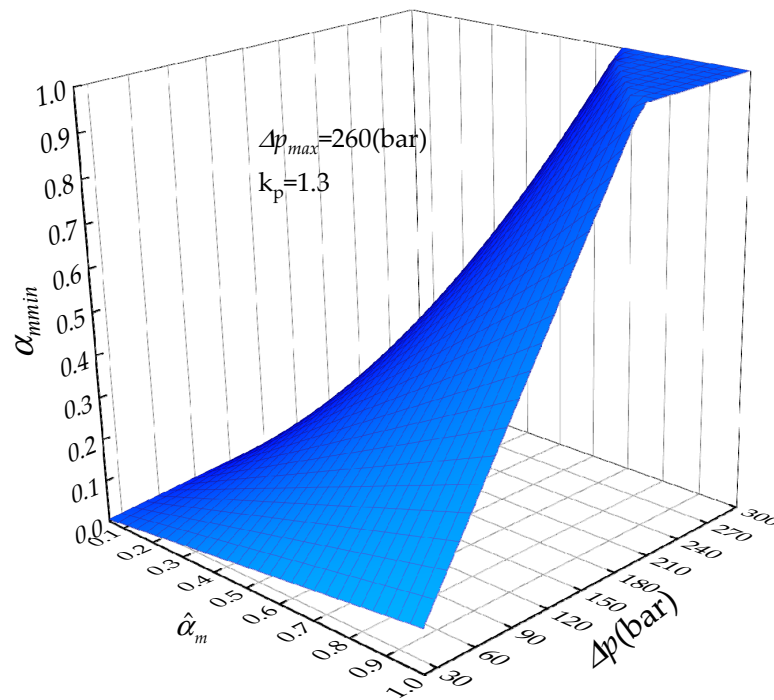


Figure 7. Variation in α_{mmin} under different values of Δp and n_e .

4. Experimental Investigation

Experimental field tests based on one THY900 heavy transport vehicle from a company were carried out to verify the effectiveness of the proposed controller. The vehicle used a closed hydrostatic powertrain (HSDP) as its travel drive system. A schematic of the HSDP system of the vehicle is shown in Figure 8a, and Figure 8c shows a photograph of the test vehicle. The HSDP system employs a driving mode in which parallel multipumps drive parallel mutimotors and the control system employs a distributed integrated control structure based on CANbus. Moreover, Dewesoft software was used to collect and record the system control and status signals. Table 1 shows basic information on the heavy transportation vehicle, and Table 2 shows the basic parameters of the main components of the vehicle's HSDP system.

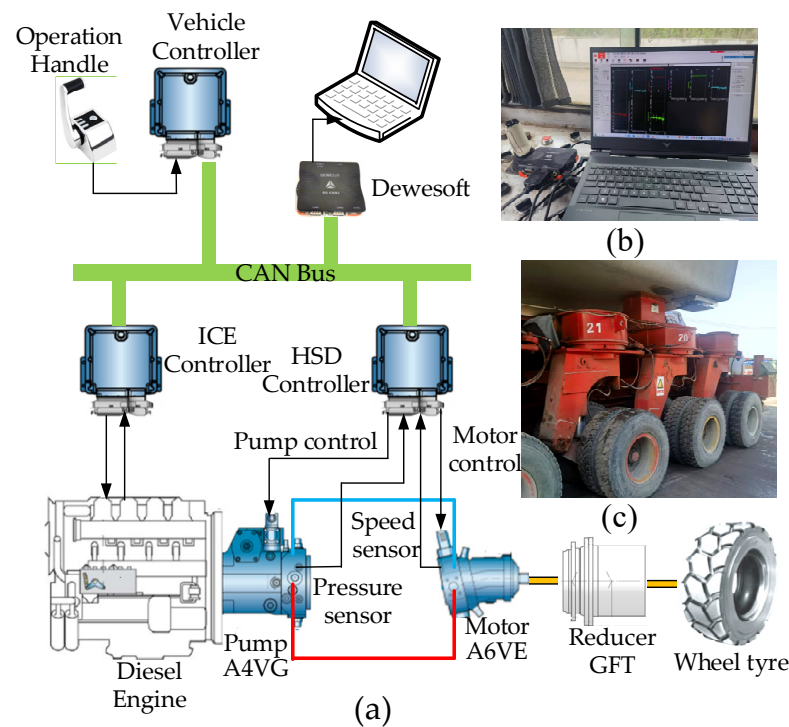


Figure 8. (a) Sketched structure of the HSDP system. (b) Scene depicting the testing of the vehicle. (c) Photograph of the test vehicle.

Table 1. Basic information on THY900 vehicle.

Vehicle	Status	Mass ($\times 10^3$ kg)	Velocity (km/h)	Motor Speed (r/min)
THY900	Empty load	300	0–10	0–3500
	Heavy load	900	0–6	0–2200

Table 2. Basic parameters of the HSDP components.

Component	Type	Parameters	Number
ICE	DEUTZ BF8M1015	Rated power: 410 kw Max speed: 2100 r/min Max torque: 2273 Nm	2
Variable pump	Rexroth A4VG250EP2	Displacement: 0–250 mL/r Rated pressure: 350 bar Control signal: 200–600 mA	4
Variable motor	Rexroth A6VE80EP2	Displacement: 0–80 mL/r Rated pressure: 350 bar Control signal: 200–600 mA	24
Reducer	Rexroth GFT36T3B79	Ratio: 79.36	24
Tire		Radius: 0.6 m	144

4.1. Testing Procedure

In this study, we tested and analyzed the speed control characteristics and adaptability to varying loads of the ADC under different travel conditions, such as no load or heavy load, driving on slopes, and driving at different travel speeds. In terms of energy saving, comparison tests between a rule-based controller (RBC) and ADC were conducted to verify the efficacy in energy saving of the ADC. A scene depicting the vehicle test is shown in Figure 8b.

Rule-Based Controller (RBC)

The control rules adopted by the RBC are widely used in commercial hydrostatic drive systems [25,34,35], in which the set speed of the engine is proportional to the reference input from the operators and the displacement of the variable pump and the variable motor are adjusted according to the engine speed and reference input. Combined with the displacement control logic of the PMDC, a rule-based controller for the vehicle was developed, and the control logic of the RBC is shown in Figure 9.

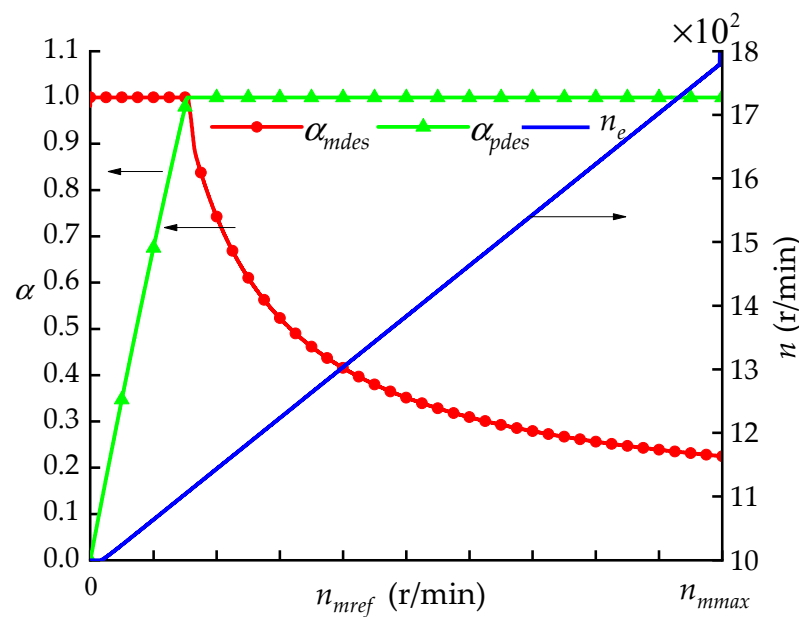


Figure 9. The commands of the rule-based controller (RBC).

The principle of the RBC is that after the RBC receives the travel commands from the operator, the engine speed increases from idle to 1000 r/min and then increases in proportion with the increase in the reference input n_{mref} . When the reference input reaches its maximum n_{mmax} (Table 1), the engine speed reaches its maximum of 1800 r/min. The control signals for the variable pump and the variable motor are determined according to the control law of PMDC.

4.2. Analysis of the Experimental Results

The performance of the ADC was analyzed comprehensively in terms of speed control, adaptability, and energy saving.

4.2.1. Characteristic of Speed Control

For spatial reasons, this paper only shows the system running states and control information in the process of the vehicle accelerating from zero to its allowable maximum speed under flat slope conditions with a heavy load and an empty load. Figure 10a shows the variation in the motor speed n_m and the reference input n_{mref} . The motor speed n_m can closely track the variation in n_{mref} and maintain good tracking accuracy. Figure 10b shows the variation process of the parameters, n_e , $\hat{\alpha}_p$, and $\hat{\alpha}_m$, and it can be seen that the three variables change cooperatively in accordance with the rules set by the ADC, thus ensuring the tracking accuracy of n_m to n_{mref} .

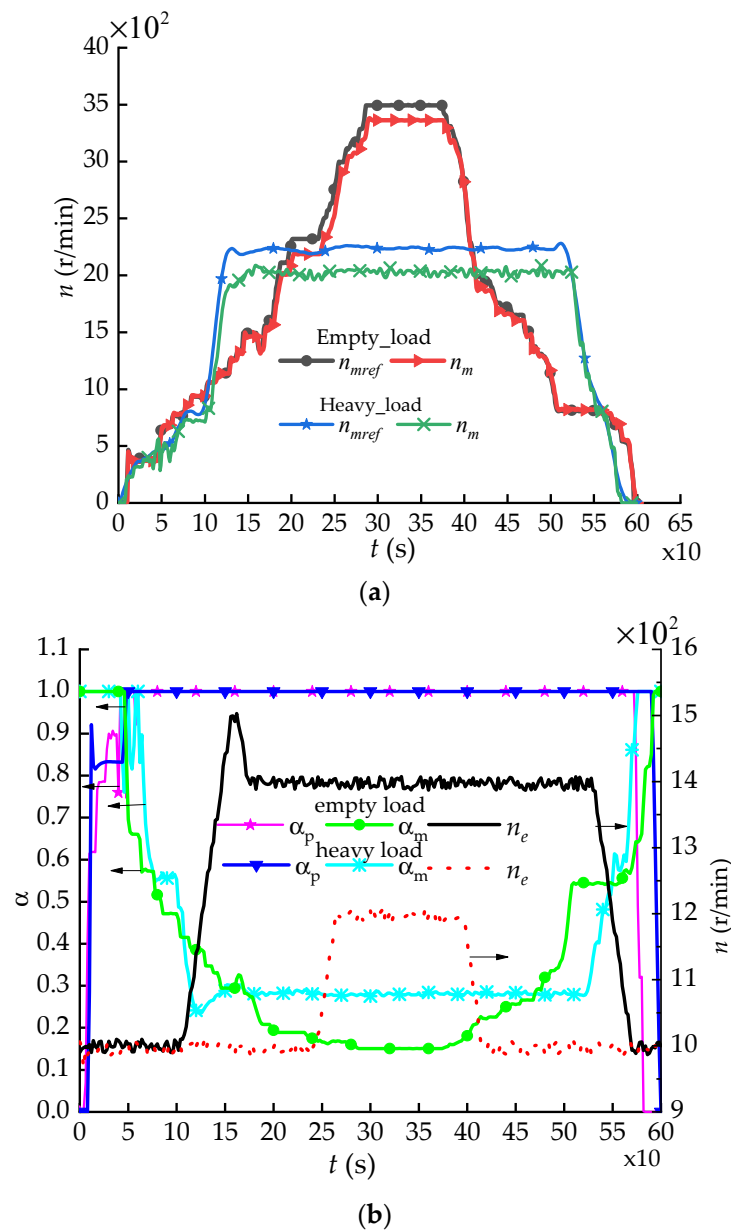


Figure 10. Operating parameter variation of the vehicle. (a) Variation in motor speeds. (b) Variation in n_e , $\hat{\alpha}_p$, and $\hat{\alpha}_m$.

A statistical analysis was conducted to analyze the speed control accuracy of the ADC. The speed control error e_n was defined as $e_n = n_{mref} - n_m$, and the average speed error ratio \bar{u} was defined as $\bar{u} = \bar{e}_n / \bar{n}_{mref}$, where \bar{e}_n is the average of e_n , and \bar{n}_{mref} is the average of n_{mref} . The statistical results are shown in Table 3.

Table 3. Statistical results regarding speed control.

Variable	Status	Max	Min	Average
n_{mref} (r/min)	Empty load	3500	0	1783
	Heavy load	2282	0	1720
e_n (r/min)	Empty load	254	−133	60
	Heavy load	397	−100	163
\bar{u} (%)	Empty load		3.3%	
	Heavy load		9.5%	

As can be seen in Table 3, the average speed error ratio of the vehicle was 3.3% under empty load conditions and 9.5% under heavy load conditions. Better speed control accuracy was achieved for the vehicle, verifying the efficacy of the ADC in speed control.

Nevertheless, there were still certain control errors for the vehicle speed under both conditions, and the errors under heavy load conditions were greater than those under empty load conditions. This phenomenon can be attributed to the reduced accuracy of the loss model of the pump and the motor caused by oil compression in the pipeline and the wear of the pumps and motors, problems that need to be addressed in future research.

4.2.2. Adaptive Characteristic

In view of the actual testing conditions for the vehicle, testing conditions of a heavy load and 2.5% slope were chosen to test the adaptability of the HSDP system. Moreover, to make the results more intuitive, the system reference input n_{mref} was always kept at its maximum value while the vehicle was climbing the slope. Figure 11a shows the variation in n_{mref} , n_m , and T_e , and Figure 11b shows the variation in $\hat{\alpha}_p$, $\hat{\alpha}_m$, and Δp during the process of vehicle climbing.

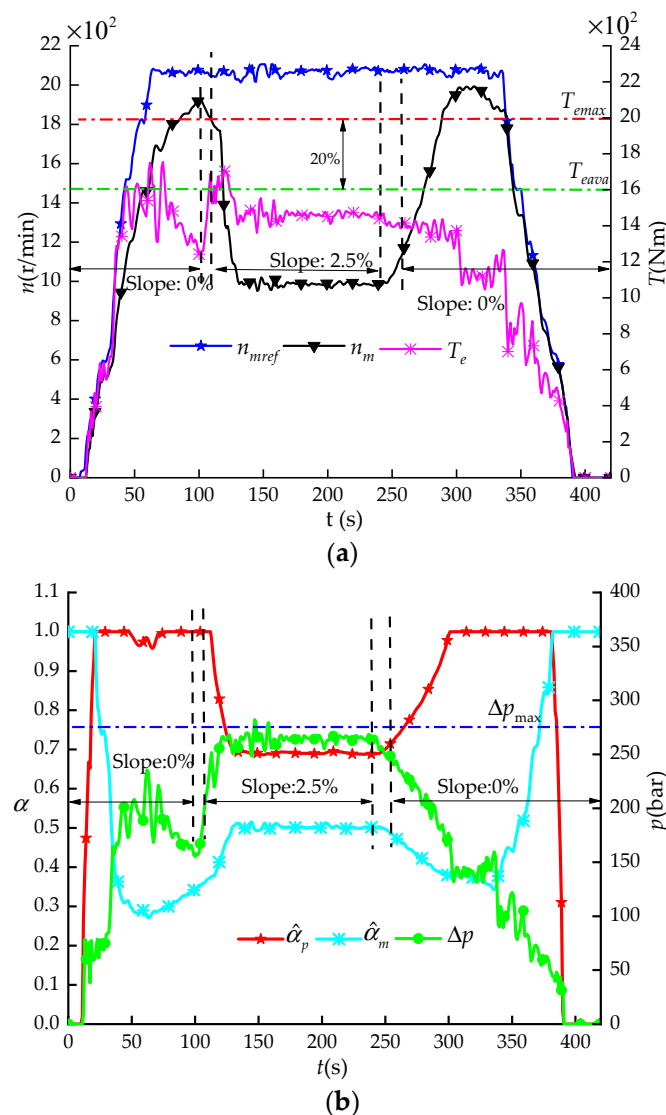


Figure 11. Variation processes of adaptive control. (a) Variation in motor speeds. (b) Variation process of Δp , $\hat{\alpha}_p$, and $\hat{\alpha}_m$.

It can be seen that when $t > 100$ s, the vehicle ascended 2.5% the slope, and the Δp and T_e began to increase. The ADC prevented the rising engine output torque T_e from exceeding its available torque T_{eava} by reducing the pump displacement ratio α_p . Meanwhile, the ADC also kept the pressure difference Δp from rising above the predefined pressure difference Δp_{max} (260 bar) by increasing the motor displacement ratio α_m . Eventually, the adaptive controller (ADC) reduced the motor speed to adapt to the increasing loads, and Δp was maintained around Δp_{max} (260 bar). When $t > 250$ s, the loads of the motor decreased as the slope decreased to zero. Then, the ADC increased the α_p and decreased the α_m automatically to align the motor speed n_m with the reference input n_{mref} again. The ADC is capable of adjusting the displacement of the pumps and motors automatically according to the vehicle loads to prevent engine stall and high system pressure, verifying the effectiveness of the ADC in terms of adaptability.

4.2.3. Energy-Saving Characteristics

The fuel consumption rate F_{cr} (L/km), i.e., the amount of fuel consumed m_f (L) per unit of traveling distance (km), was chosen as the measuring unit to evaluate the fuel economy of the engine to reduce the impact of the difference in instantaneous fuel consumption and speed control errors on the evaluation results. Comparison tests between the ADC and RBC were carried out under different conditions. However, for ease of analysis, only the statistical results obtained for a flat slope (0%) are given, which are shown in Table 4.

Table 4. The comparative results of RBC and ADC.

Status		Adaptive Controller (ADC)					Rule-Based Controller (RBC)		
Slope (%)	Mass ($\times 10^3$ kg)	Velocity (km/h)	Distance (m)	m_f (L)	F_{cr} (L/km)	ΔF_{cr} (%)	Distance (m)	m_f (L)	F_{cr} (L/km)
0	300	2	213.6	1.27	5.95	−25.8	221.4	1.77	8.02
		4	405	1.63	4.04	−26.3	440	2.41	5.48
		6	579.7	2.06	3.55	−24.0	662.1	3.09	4.67
		8	776.0	2.64	3.40	−19.8	887.9	3.77	4.24
		10	977.3	3.26	3.34	−11.4	1117.5	4.22	3.77
	900	1	99.6	1.57	15.76	−9.0	98.4	1.70	17.31
		2	204.0	2.22	10.88	−4.7	203.3	2.32	11.42
		3	306.0	3.21	10.48	−5.5	296	3.28	11.09
		5	511.6	5.49	10.72	−2.8	475.6	5.25	11.03
		6	590.6	6.96	11.79	−3.5	580.0	7.09	12.22

As shown in Table 4, the fuel consumption rate F_{cr} of the ADC was lower than that of the RBC under both heavy load and empty load conditions. Specifically, the energy-saving ratio ΔF_{cr} was at least 11.4% and up to 25.8% under empty load conditions and at least 2.8% and up to 9% under heavy load conditions. The decreasing fuel consumption rate F_{cr} is proof of the effectiveness of the ADC in energy saving.

Additionally, the results of the comparison tests under other conditions are presented in the form of a scatter plot of the engine operating points in Figure 12.

It can be seen from Figure 12 that the engine operating points under the control of the rule-based controller (RBC) are more dispersed than those under the adaptive controller (ADC), which shows that the engine operating points of the RBC are easily affected by changes in the vehicle power. With the increase in power, the engine operating points become closer to the optimal operating line (OOL). However, the engine operating points of the ADC are more concentrated around the OOL than those of RBC, especially when the vehicle power is below 150 kw. When the power is above 150 kw, they become further away from the OOL as power increases but still remain closer to the OOL than those of the RBC, which indicates that the engine operating points of the ADC are less influenced by changes in the vehicle power. The optimal operating line (OOL) of the engine is drawn based on the principle of the minimum BSFC under certain operating points of the engine,

with greater energy savings at points closer to the OOL. Therefore, the ADC performed better in terms of energy saving than the RBC during most of the driving conditions.

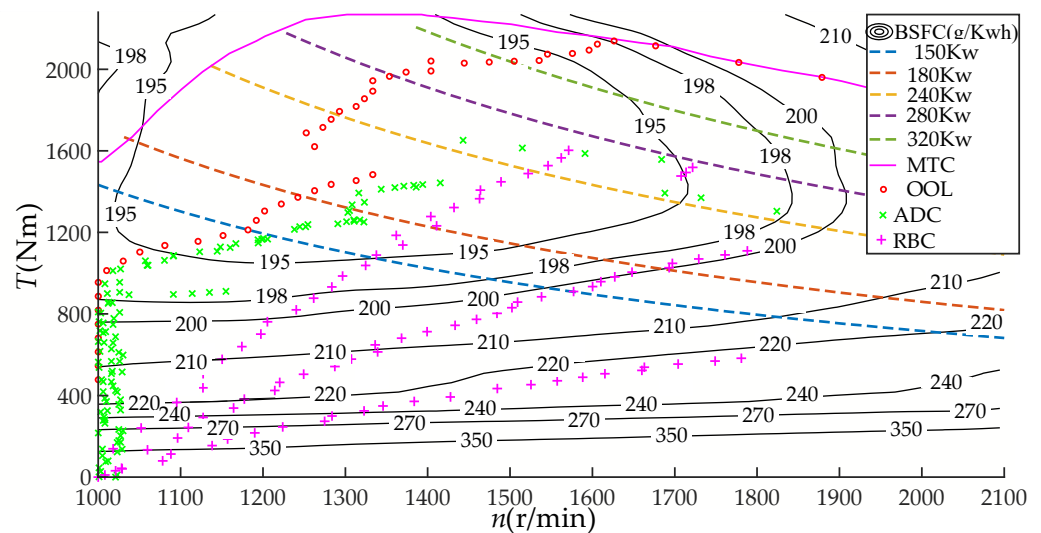


Figure 12. Scatter plot of engine operating points.

5. Discussions and Future Work

Although the accuracy of the speed control satisfies the requirements of heavy transportation vehicles, it is still not a satisfactory result. The accuracy of the speed control of the proposed ADC is easily affected by the load conditions of the vehicle, which can be attributed to the semiclosed loop speed control method based on the established loss models. The loss models of the pump and the motor ignore the oil compression and the wear of the pumps and motors, which decreases the accuracy of the loss models to some extent. Therefore, in future research, a full closed-loop speed control strategy will be investigated and integrated into the control system to compensate for the modeling error of the loss models, thus further improving the speed control accuracy. Moreover, while the energy-saving effect of the ADC was validated using the reported tests, it cannot ensure the optimal performance in all driving situations, especially in driving conditions involving rapidly changing loads. Additionally, the BSFC curves of the engine were only tested under steady-state conditions, which will cause increased fuel consumption in dynamic situations. In the future, model-based control strategies, which consider the dynamic effect of the HSDP system, will be investigated to provide better overall fuel economy.

6. Conclusions

Focusing on a closed hydrostatic powertrain (HSDP) composed of an engine, a variable pump, and a variable motor, this paper proposes an energy-efficient adaptive speed-regulating controller (ADC) based on power following. As well as ensuring accurate speed control through online system efficiency estimation based on the pump/motor loss model and the system feedback signal, this controller can also seek the optimal efficiency control of the engine and the hydrostatic system through the two redundant control freedoms of the HSDP system. Meanwhile, the controller can prevent engine overload stall and high system pressure by limiting the displacement of the pumps and motors based on the loads of the system in real time to improve the automatic adaptability of the system to varying loads. Experimental field tests based on a heavy transportation vehicle were carried out to verify the efficacy of the ADC in terms of speed control accuracy and adaptability. Moreover, tests comparing a rule-based controller (RBC) and the ADC were also conducted to validate the energy-saving effect of the ADC. The field experimental results indicate the following:

1. The ADC can allow the motor speed to accurately track changes in the reference and maintain an accuracy with an average error of 3.3% under empty load conditions and 9.5% under heavy load conditions.
2. The ADC reduces motor speed automatically through the displacement adjustment of the pumps and the motors to allow the HSDP system to adapt to rising loads, thus preventing engine overload stall and high system pressure.
3. Compared to the RBC, the energy-saving ratio of the ADC is at least 11.4% and up to 25.8% under empty load conditions and at least 2.8% and up to 9% under heavy load conditions, showing the significant energy-saving effect of the ADC.

Author Contributions: Conceptualization, H.W. and R.L.; methodology, H.W.; software, H.W.; validation, H.W., Z.A. and Y.Z.; formal analysis, H.W.; investigation, H.W.; resources, H.W. and Z.A.; data curation, H.W. and R.L.; writing—original draft preparation, H.W.; writing—review and editing, H.W. and Y.Z.; visualization, Y.Z.; project administration, Y.Z. All authors have read and agreed to the published version of the manuscript.

Funding: This research is supported by the Key Scientific and Technological Project of Henan Province (No.232102220044), the Science and Technology Research Project of the Science and Technology Department from Henan Province (No. 212102210225), and the 2023 Science and Technology Development Plan Project of China Railway 11th Bureau Group Co., LTD (No. 23-AII-08).

Data Availability Statement: All data used in this manuscript can be made available upon request.

Acknowledgments: The test vehicle and test sites are provided by the 3rd Engineering Co., Ltd., China Railway 11th Bureau Group.

Conflicts of Interest: Zhangshun An was employed by China Railway 11 Bureau Group. The remaining authors declare that the research was conducted in the absence of any commercial or financial relationships that could be constructed as a potential conflict of interest.

References

1. Yang, X.; Gong, G.; Yang, H.; Jia, L.; Zhou, J. An investigation in performance of a variable speed displacement pump-controlled motor system. *IEEE/ASME Trans. Mechatron.* **2017**, *22*, 647–656. [\[CrossRef\]](#)
2. Sakaino, S.; Sakuma, T.; Tsuji, T. A control strategy for electro-hydrostatic actuator considering static friction, resonance, and oil Leakage. *IEEE J. Ind. Appl.* **2019**, *8*, 279–286. [\[CrossRef\]](#)
3. Shi, H.; Yang, H.; Gong, G.; Liu, H.; Hou, D. Energy saving of cutterhead hydraulic drive system of shield tunneling machine. *Autom. Constr.* **2014**, *37*, 11–21. [\[CrossRef\]](#)
4. Zhang, Q.; Wang, F.; Cheng, M.; Xu, B. Energy efficiency improvement of battery powered wheel loader with an electric-hydrostatic hybrid powertrain. *Proc. Inst. Mech. Eng. Part D J. Automob. Eng.* **2022**, *237*, 75–88. [\[CrossRef\]](#)
5. Li, Y.; He, L. Counterbalancing speed control for hydrostatic drive heavy vehicle under long down-slope. *IEEE/ASME Trans. Mechatron.* **2015**, *20*, 1533–1542. [\[CrossRef\]](#)
6. Wang, F.; Wu, Z.; Xu, B.; Fiebig, W. A mode-driven control strategy to reduce electric drive peak power of hybrid wheel loader propulsion system. *IEEE Trans. Veh. Technol.* **2023**, *72*, 5948–5961. [\[CrossRef\]](#)
7. Bender, F.; Kaszynski, M.; Sawodny, O. Drive cycle prediction and energy management optimization for hybrid hydraulic vehicles. *IEEE Trans. Veh. Technol.* **2013**, *62*, 3581–3592. [\[CrossRef\]](#)
8. Hippalgaonkar, R.; Ivantysynova, M. Optimal power management of hydraulic hybrid mobile machines—Part I: Theoretical studies, modeling and simulation. *J. Dyn. Syst. Meas. Control* **2016**, *138*, 100201–100223. [\[CrossRef\]](#)
9. Kim, H.; Yoo, S.; Cho, S.; Yi, K. Hybrid control algorithm for fuel consumption of a compound hybrid excavator. *Autom. Constr.* **2016**, *68*, 1–10. [\[CrossRef\]](#)
10. Kwon, H.; Ivantysynova, M. Experimental and theoretical studies on energy characteristics of hydraulic hybrids for thermal management. *Energy* **2021**, *223*, 120033. [\[CrossRef\]](#)
11. Ge, L.; Quan, L.; Zhang, X.; Dong, Z.; Yang, J. Power matching and energy efficiency improvement of hydraulic excavator driven with Speed and displacement variable power source. *Chin. J. Mech. Eng.* **2019**, *32*, 100. [\[CrossRef\]](#)
12. Sun, H.; Yang, L.F.; Jing, J.Q. Hydraulic/electric synergy system (HESS) design for heavy hybrid vehicles. *Energy* **2010**, *35*, 5328–5335.
13. Ge, L.; Quan, L.; Zhang, X.; Zhao, B.; Yang, J. Efficiency improvement and evaluation of electric hydraulic excavator with speed and displacement variable pump. *Energy Convers. Manag.* **2017**, *150*, 62–71. [\[CrossRef\]](#)
14. Yan, Z.; Ge, L.; Quan, L. Energy-efficient electro-hydraulic power source driven by variable-speed motor. *Energies* **2022**, *15*, 4804. [\[CrossRef\]](#)

15. Wang, F.; Hong, J.Y.; Ding, R.Q.; Xu, B.; Fiebig, W.J. A torque conversion solution to the powertrain of mobile machine and its control strategy. *IEEE Trans. Veh. Technol.* **2022**, *71*, 10361–10373. [[CrossRef](#)]
16. He, X.; Liu, H.; He, S.; Hu, B.; Xiao, G. Research on the energy efficiency of energy regeneration systems for a battery-powered hydrostatic vehicle. *Energy* **2019**, *178*, 400–418. [[CrossRef](#)]
17. Castaings, A.; Lhomme, W.; Trigui, R.; Bouscayrol, A. Comparison of energy management strategies of a battery/supercapacitors system for electric vehicle under real-time constraints. *Appl. Energy* **2016**, *163*, 190–200. [[CrossRef](#)]
18. Froehlich, C.; Kemmetmuller, W.; Kugi, A. Model predictive control of servo-pump driven injection molding machines. *IEEE Trans. Control Syst. Technol.* **2020**, *28*, 1665–1680. [[CrossRef](#)]
19. Deppen, T.O.; Alleyne, A.G.; Meyer, J.J.; Stelson, K.A. Comparative study of energy management strategies for hydraulic hybrids. *J. Dyn. Syst. Meas. Control* **2015**, *137*, 041002. [[CrossRef](#)]
20. Zhang, Q.; Wang, F.; Xu, B.; Sun, Z. Online optimization of Pontryagin’s minimum principle for a series hydraulic hybrid wheel loader. *Proc. Inst. Mech. Eng. Part D J. Automob. Eng.* **2021**, *236*, 1487–1499. [[CrossRef](#)]
21. Jung, D.; Cho, S.W.; Park, S.J.; Min, K.D. Application of a modified thermostatic control strategy to parallel mild HEV for improving fuel economy in urban driving conditions. *Int. J. Automot. Technol.* **2016**, *17*, 339–346. [[CrossRef](#)]
22. Wen, Q.Y.; Wang, F.; Xu, B.; Sun, Z. Improving the fuel efficiency of compact wheel loader with a series hydraulic hybrid powertrain. *IEEE Trans. Veh. Technol.* **2020**, *69*, 10700–10709. [[CrossRef](#)]
23. Do, H.T.; Park, H.G.; Ahn, K.K. Application of an adaptive fuzzy sliding mode controller in velocity control of a secondary controlled hydrostatic transmission system. *Mechatronics* **2014**, *24*, 1157–1165. [[CrossRef](#)]
24. Backas, J.; Ghabcheloo, R.; Tkkanen, S.; Huhtala, K. Fuel optimal controller for hydrostatic drives and real-world experiments on a wheel loader. *Int. J. Fluid Power* **2016**, *17*, 187–201. [[CrossRef](#)]
25. Zhao, J.Y.; Wang, Z.Y.; Qin, Y.M.; Wang, J.X. Research on the hydraulic driving system and engine power match in TLC900 transporting grider vehicle. *Chin. J. Mech. Eng.* **2007**, *18*, 878–881.
26. Ye, H.; Ni, X.; Chen, H.; Li, D.; Pan, W. Constant speed control of hydraulic travel system based on neural network algorithm. *Processes* **2022**, *10*, 944. [[CrossRef](#)]
27. Zeng, X.; Li Ly Song, D.; Li, L.; Li, G. Model predictive control based on time-varying efficiency for hydraulic hub-motor driving vehicle. *Proc. Inst. Mech. Eng. Part D J. Automob. Eng.* **2021**, *235*, 2949–2963. [[CrossRef](#)]
28. Xu, B. Characteristics of volumetric losses and efficiency of axial piston pump with respect to displacement conditions. *J. Zhejiang Univ. Sci. A* **2016**, *17*, 186–201. [[CrossRef](#)]
29. Tan, Y.; Yu, X.; Wang, X.; Lv, Q.; Shi, M. Interaction analysis and multi-response optimization of transformer winding design parameters. *Int. Commun. Heat Mass Transf.* **2022**, *137*, 106233. [[CrossRef](#)]
30. Keller, N.; Ivantysynova, M. A new approach to sizing low pressure systems. In Proceedings of the ASME/BATH 2017 Symposium on Fluid Power & Motion Control, Sarasota, FL, USA, 16–19 October 2017.
31. Vardhan, A.; Dasgupta, K. Mapping the efficiency of the hydrostatic drive for the rotary head of drill machine using high-speed low-torque hydraulic motors. *Arab. J. Sci. Eng.* **2018**, *43*, 4703–4712. [[CrossRef](#)]
32. Manring, N.D. Mapping the efficiency for a hydrostatic transmission. *J. Dyn. Syst. Meas. Control* **2016**, *138*, 031004. [[CrossRef](#)]
33. Pandey, A.K.; Vardhan, A.; Dasgupta, K. Theoretical and experimental studies of the steady-state performance of a primary and secondary-controlled closed-circuit hydrostatic drive. *Proc. Inst. Mech. Eng. Part E J. Process Mech. Eng.* **2019**, *233*, 1024–1035. [[CrossRef](#)]
34. Bosch Rexroth, A.G. *Easy Machine Operation with Rexroth Automotive Drive and Anti-Stall Control*; Bosch Group: Elchingen, Germany, 2003.
35. Eaton Corporation. *ETAC: Electronic Transmission Automotive Control User’s Manual*; Eaton Corporation: Eden Prairie, MN, USA, 2007.

Disclaimer/Publisher’s Note: The statements, opinions and data contained in all publications are solely those of the individual author(s) and contributor(s) and not of MDPI and/or the editor(s). MDPI and/or the editor(s) disclaim responsibility for any injury to people or property resulting from any ideas, methods, instructions or products referred to in the content.